

Gold nanoparticles/single-stranded DNA-reduced graphene oxide nanocomposites based electrochemical biosensor for highly sensitive detection of cholesterol

Shuyao Wu¹, Chengquan Sui¹, Chong Wang¹, Yulu Wang¹, Dongqing He¹, Ying Sun¹, Yu Zhang¹, Qingbo Meng¹,
Tianyi Ma (✉)², Xi-Ming Song (✉)¹

¹ Liaoning Key Laboratory for Green Synthesis and Preparative Chemistry of Advanced Materials, College of Chemistry, Liaoning University, Shenyang 110036, China

² Centre for Translational Atomaterials, Swinburne University of Technology, Hawthorn VIC 3122, Australia

© Higher Education Press 2021

Abstract High density and uniform distribution of the gold nanoparticles functionalized single-stranded DNA modified reduced graphene oxide nanocomposites were obtained by non-covalent interaction. The positive gold nanoparticles prepared by phase inversion method exhibited good dimensional homogeneity and dispersibility, which could readily combine with single-stranded DNA modified reduced graphene oxide nanocomposites by electrostatic interactions. The modification of single-stranded DNA endowed the reduced graphene oxide with favorable biocompatibility and provided the preferable surface with negative charge for further assembling of gold nanoparticles to obtain gold nanoparticles/single-stranded DNA modified reduced graphene oxide nanocomposites with better conductivity, larger specific surface area, biocompatibility and electrocatalytic characteristics. The as-prepared nanocomposites were applied as substrates for the construction of cholesterol oxidase modified electrode and well realized the direct electron transfer between the enzyme and electrode. The modified gold nanoparticles could further catalyze the products of cholesterol oxidation catalyzed by cholesterol oxidase, which was beneficial to the enzyme-catalyzed reaction. The as-fabricated bioelectrode exhibited excellent electrocatalytic performance for the cholesterol with a linear range of 7.5–280.5 $\mu\text{mol}\cdot\text{L}^{-1}$, a low detection limit of 2.1 $\mu\text{mol}\cdot\text{L}^{-1}$, good stability and reproducibility. Moreover, the electrochemical biosensor showed good selectivity and acceptable accuracy for the detection of cholesterol in human serum samples.

Keywords reduced graphene oxide, gold nanoparticles, electrochemical biosensor, cholesterol oxidase, cholesterol

1 Introduction

Cholesterol and its fatty acids are very important for human body, which are the formation of biofilms, and the structural components of nerve and brain cells [1,2]. When the cholesterol levels in serum are excessively high, the incidence rate of blood vessel damage and a series of fatal diseases such as hypertension, arteriosclerosis, lipid metabolism disorders and cerebral thrombosis, etc. will be increased [3,4]. High cholesterol can also cause the diseases such as diabetes, kidney disease, jaundice and cancer [5]. For the diagnosis of the above serious diseases, the determination of the cholesterol level in the blood is one of the important indicators [6]. Gas chromatography, high-performance liquid chromatography and spectrophotometry are the traditional methods of cholesterol detection [7–9]. However, these methods have disadvantages such as high labor intensity, complicated operation procedures, poor selectivity and high cost. Electrochemical techniques remain the better favorable choice, due to their unbeaten virtues like sensitivity, cost effectiveness, quick response and ease of operation [10–12]. Lately, many materials have been used to fabricate new types of cholesterol electrochemical biosensors [13,14].

Colloidal gold nanoparticles (AuNPs), characterized by large specific surface area, better biocompatibility, and low electron transfer resistance, have been widely used in many fields from interface interaction studies to biosensors [15–17]. For example, Han et al. [18] used AuNPs and molybdenum disulfide/graphene modified electrodes to develop a nitrite ions electrochemical sensor with high

Received June 3, 2021; accepted September 2, 2021

E-mails: tianyima@swin.edu.au (Ma T),
songlab@lnu.edu.cn (Song X-M)

sensitivity and good stability. Kumar-Krishnan et al. [19] prepared amine groups functionalized AuNPs on the silicon dioxide. The hybrid not only increased the immobilized amount of glucose oxidase (GOx), but also well maintained the biological activity of GOx and promoted the electron transfer rate between enzyme and the electrode. At present, the research of AuNPs in electrochemical biosensing mostly focused on the negatively charged gold nanoparticles (AuNPs⁻), and there are few studies on the positive charged AuNPs (AuNPs⁺). In fact, AuNPs⁺ prepared in organic solvents are better than AuNPs⁻ in aqueous solution in terms of the monodispersity, and their size and shape can be pre-designed, furthermore, the concentration of nanogolds produced is relatively high [20]. To preferably stabilize AuNPs, prevent them from agglomerating and further increase their electrical conductivity, carbon-based nanomaterials were frequently used to composite with them as the appropriate supporter [21,22].

Graphene has outstanding characteristics of excellent electrical conductivity, high theoretical specific surface area, good thermal conductivity, etc. [23], which have become the research hotspots in many fields recently, and their application in the aspect of modern electrochemical analysis has been increasingly paid attentions [24]. Compared with other carbon-based nanomaterials, graphene-based nanomaterials modified electrodes have shown better electrochemical performance and become one of the popular materials in the field of electrochemical sensing research [25,26]. Using graphene as the electrode material cannot only greatly promote the electron transfer rate, but also increase the specific surface area of the electrode, which is benefit to the electrochemical sensing performance of the modified electrodes to achieve efficient detection for target molecules [27,28]. However, owing to the aromatic indefinite system composed of carbon atoms in the graphene framework, there is a strong van der waals force between the graphene sheets, leading to their irreversible aggregation in aqueous solutions and poor compatibility to biomolecules. Therefore, functionalizing graphene with good dispersability in water and biocompatibility is particularly important for their further application in electrochemical biosensing. The optimization design of functionalized materials and methods is important for endowing graphene with better performance. Graphene composites modified by the non-covalent methods have the obvious advantage of maintaining the original structure of graphene without being damaged while introducing functional groups with novel properties and functions [29]. DNA molecules can interact with the surface of the graphene nanosheets by the non-covalent π - π interaction through their purine and pyrimidine bases structure [30]. The sugar phosphate backbone of the DNA can form a hydrophilic outer layer toward the surface away from the graphene [31], which can effectively improve the

dispersibility in aqueous medium. Our group has successfully prepared the single-stranded DNA (ssDNA) modified graphene nanocomposite with good biocompatibility for the immobilization of horseradish peroxidase, showing good catalytic detection performance for hydrogen peroxide (H₂O₂) [32].

In this paper, the positively charged AuNPs were prepared by phase inversion method with good dimensional homogeneity and dispersibility, which could readily combine with ssDNA modified reduced graphene oxide (rGO). The modification of ssDNA endowed the rGO with good biocompatibility and water-dispersibility, meanwhile exhibited significant negative charge property, which provided preconditions for further assembling of AuNPs. The AuNPs could be evenly dispersed on the ssDNA-rGO nanosheets under the electrostatic interaction to produce AuNPs/ssDNA-rGO ternary nanocomposites. The combination of ssDNA, rGO and AuNPs made full advantages of the each, so that the nanocomposites possessed better conductivity, a larger specific surface area and biocompatibility. The AuNPs/ssDNA-rGO nanocomposites were used as the substrates for immobilizing the cholesterol oxidase (ChOx), and the fabricated biosensing interface exhibited good electrochemical catalysis performance for the cholesterol detection.

2 Experimental

2.1 Materials

Salmon sperm DNA, HAuCl₄·3H₂O, ChOx (EC 1.1.3.6, 500U) and cholesterol esterase (ChEt, EC 3.1.1.13, 10U) were provided from Sigma-Aldrich Chemical Co., Ltd. Hydrazine hydrate solution (85 wt-%), high-purity graphite powder, K₄Fe(CN)₆, cholesterol, ethanol, acetone and NaOH, isopropyl alcohol were purchased from Sinopharm Chemical Reagent Co. Ltd. NaBH₄, KMnO₄, H₂SO₄ and KCl were supplied by Tianjin Yongda Chemical Reagent Co., Ltd. Tetraoctylammonium bromide, 4-dimethylaminopyridine and K₃Fe(CN)₆ were obtained from Aladdin Biochemical Technology Co., Ltd. Triton X-100, isopropanol, ascorbic acid (AA), glucose (Glu), uric acid (UA) and lactic acid (LA) were obtained from Alfa Aesar. All the other reagents were analytical grade and used without further purification. A stock solution of 0.1 mmol·L⁻¹ cholesterol was prepared in 0.1 mol·L⁻¹ phosphate-buffered saline (PBS, pH 6.5) containing 0.5% (v/v) isopropanol and 0.2% (v/v) Triton X-100 in a bath at 60 °C. The cholesterol solution was stored at 4 °C when not in use.

2.2 Preparation of the ssDNA-rGO nanocomposites

Typically, 120 mg of salmon sperm DNA was added into

20 mL of deionized water, and refluxed at 95 °C for 2 h to obtain a light yellow homogeneous solution, which was 6 mg·mL⁻¹ of ssDNA dispersion [33].

GO was prepared by the Hummer method [34]. Brownish yellow GO (100 mg) was added into 20 mL of deionized water, ultrasonically dispersed for 3 h to obtain a brown homogeneous solution. The ssDNA dispersion prepared above (20 mL) was mixed with an equal volume of GO dispersion and heated under stirring for 30 min. Then, 0.1 mL of hydrazine hydrate was added, and the mixture was refluxed at 100 °C for 4 h. Then, the reaction liquid was centrifuged at 12000 r·min⁻¹ for 5 min, washed with deionized water, and the process was repeated three times in order to remove the excessed hydrazine hydrate and free ssDNA, finally the ssDNA-rGO nanocomposites were obtained.

2.3 Preparation of AuNPs[®]

AuNPs[®] was prepared according to the literature [35] with minor improvements. First, 1 mL of 1% chloroauric acid solution and 2.5 mL of freshly prepared *tetra-n*-octyl ammonium bromide toluene solution (25 mmol·L⁻¹) were added in a small beaker, and magnetically stirred for 30 min to completely transfer HAuCl₄ from the aqueous phase to the toluene phase. The upper liquid was observed to be orange quickly. Then, 8.3 mL of fresh sodium borohydride solution (0.04 mol·L⁻¹) was fleetly added into the mixed liquor. The upper orange solution turned into wine red instantly and was continuously stirred for 30 min. After standing to the layers stratified, the lower layer of liquid was separated, and the toluene layer was washed three times with 0.1 mol·L⁻¹ H₂SO₄, 0.1 mol·L⁻¹ NaOH and twice with water, respectively. The freshly prepared 4-dimethylaminopyridine was added to the toluene layer in an equal volume. It was observed that the deep wine colloid was transferred from the toluene phase to the aqueous phase and allowed to stand for about 1 h. After the AuNPs in the toluene layer were completely transferred to the lower layer solution, the two phases were separated to retain the lower layer liquid, that was, the positively charged AuNPs were obtained and stored in a refrigerator at 4 °C.

2.4 Preparation of the AuNPs/ssDNA-rGO nanocomposites

The AuNPs dispersion and 1 mg·mL⁻¹ ssDNA-rGO were mixed in equal volume, and sonicated for 15 min to obtain a uniform black dispersion, and then centrifuged (8000 r·min⁻¹, 5 min) four times to remove the free AuNPs, then AuNPs/ssDNA-rGO nanocomposites were obtained.

2.5 Fabrication of the ChOx/AuNPs/ssDNA-rGO/GCE

Prior to use, the glassy carbon electrode (GCE) was

polished with Al₂O₃ slurry to obtain a mirror-like surface and sonicated in ethanol and ultrapure water, respectively, then the electrode was dried with nitrogen flow. After that, 5 μL aqueous solution of AuNPs/ssDNA-rGO (1 mg·mL⁻¹) was dropped on the GCE. After the water was dried out, the AuNPs/ssDNA-rGO thin film was formed on the surface of electrode, and the AuNPs/ssDNA-rGO/GCE was obtained. Then the modified electrode was immersed into ChOx solution (5 mg·mL⁻¹, pH 4.0 PBS) at 4 °C for 24 h in order to adequately adsorbed the ChOx. After that, ChOx/AuNPs/ssDNA-rGO/GCE was obtained. For comparison, the fabricated procedure of ssDNA-rGO/GCE, AuNPs/ssDNA-rGO/GCE and ChOx/ssDNA-rGO/GCE were similar to that of ChOx/AuNPs/ssDNA-rGO/GCE. The modified electrodes were preserved under the condition of 4 °C in the refrigerator before use.

2.6 Electrochemical measurements

A traditional three-electrode system was used in electrochemical experiment. Ag/AgCl electrode was served as the reference electrode, Pt wire as the counter electrode and the modified GCE as the working electrode. Before the electrochemical tests, the working electrode was washed by ultra-pure water to remove the nonspecific adsorbed ChOx and the high purity nitrogen was purged to 10 mL of 0.1 mol·L⁻¹ PBS (pH 6.5) for 30 min to remove the dissolved oxygen. In the electrochemical catalysis experiment, the oxygen was purged to the PBS until saturation.

In the electrochemical impedance spectroscopy test, the nyquist plots were measured at frequency range of 0.1 Hz–100 kHz. The alternating voltage is 5 mV. The test solution was K₃[Fe(CN)₆]/K₄[Fe(CN)₆] solution with a concentration of 5.0 mmol·L⁻¹ containing 0.1 mol·L⁻¹ KCl. The parameters of differential pulse voltammetry (DPV) were set as follows: the scanning interval was -0.1–0.7 V, and the amplitude was 50 mV.

2.7 Apparatus

The morphology of AuNPs/ssDNA-rGO nanocomposites were observed using a model JEM-2100 transmission electron microscope (TEM, Hitachi Corp., Japan). The crystalline structure was recorded by a Powder D8 Advance X-ray diffraction (XRD, Bruker Corp., USA) with CuKα radiation (0.15418 nm). Ultraviolet-visible (UV-vis) spectra were collected utilizing a Lambda 35 spectrophotometer (Perkin Elmer Corp., USA). Zeta potential data were measured using a Zetasizer Nano-ZS particle analyzer (Malvern Corp., UK). Electrochemical impedance spectroscopy, cyclic voltammogram (CV) and DPV measurements were performed using a CHI660E electrochemical workstation (Shanghai Chenhua Instruments Co., China).

3 Results and discussion

3.1 Characterization of the AuNPs/ssDNA-rGO nanocomposites

The morphology of the nanocomposites was characterized by TEM. The images of AuNPs (a), ssDNA-rGO (b) and AuNPs/ssDNA-rGO (c) are shown in Fig. 1. Figure 1(a) showed that the diameter of AuNPs ranges from 1.0 to 7.0 nm with good monodispersity. After the bright brown GO was reduced and modified by ssDNA, the ssDNA-rGO turned black with well aqueous dispersity (Fig. 1(d)) and appeared typical morphology of the rGO nanosheet, as shown in Fig. 1(b). When modified on the surface of ssDNA-rGO nanocomposites, the AuNPs were dispersed uniformly on the ssDNA-rGO sheets (Fig. 1(c)), with only a very small number of AuNPs agglomerating and no scattered ones around. It might be related to the preferred prepared method of AuNPs and the stabilized ability of ssDNA-rGO. The AuNPs/ssDNA-rGO nanocomposite also presented good aqueous dispersity and no agglomeration unlike the unmodified rGO (Fig. 1(d)).

Zeta potential is considered to be an important parameter for evaluating the stability of dispersion systems. When the zeta potential value of the colloidal system is greater than ± 30 mV, the system can stably disperse [36]. The AuNPs prepared by the phase transfer method had a zeta potential of 34.5 mV (Fig. 1(e-i)). Since the AuNPs were covered by 4-methylaminopyridine with a positive amino functional group on their surface, the AuNPs had significant positive charges on their surface. The zeta potential of ssDNA-rGO

was measured to be -41.9 mV (Fig. 1(e-ii)), with significant negative charges on their surface. Due to the significant difference in charge properties and zeta potentials between AuNPs and ssDNA-rGO, that they had a good interaction during the assembled process. The zeta potential of the AuNPs/ssDNA-rGO nanocomposite was -32.6 mV (Fig. 1(e-iii)).

The UV-Vis spectrogram and XRD patterns of the different materials are shown in Fig. 2. The UV-Vis spectra of GO, ssDNA-rGO, ssDNA and AuNPs/ssDNA-rGO aqueous dispersions are represented in Fig. 2(a). As shown in curve (i), the characteristic peak of GO presented at 230 nm. When GO was reduced by hydrazine hydrate, the characteristic peak redshifted to 270 nm (curve (ii)) due to the increase in the π - π conjugated system, indicating that GO was reduced. The absorption peak of curve (iii) at 260 nm was the characteristic absorption of the ssDNA. When AuNPs were modified on the rGO surface, two new peaks appeared on the curve (iv). The characteristic absorption peak of pyridine ring in 4-methylaminopyridine covering on the surface of AuNPs at 249 nm and the AuNPs at 530 nm were observed (The inner illustration was the magnification of the absorption peak of AuNPs. This showed that the AuNPs were successfully loaded on ssDNA-rGO nanosheets [37].

The crystal structure of the nanohybrid was further characterized by XRD. As can be seen in Fig. 2(b), the (001) peak of GO appeared at 11.3° . When GO was reduced, the characteristic peak of ssDNA-rGO exhibited a wide graphite (002) crystal plane diffraction peak at 26.5° , illustrating the modification of ssDNA had a certain effect

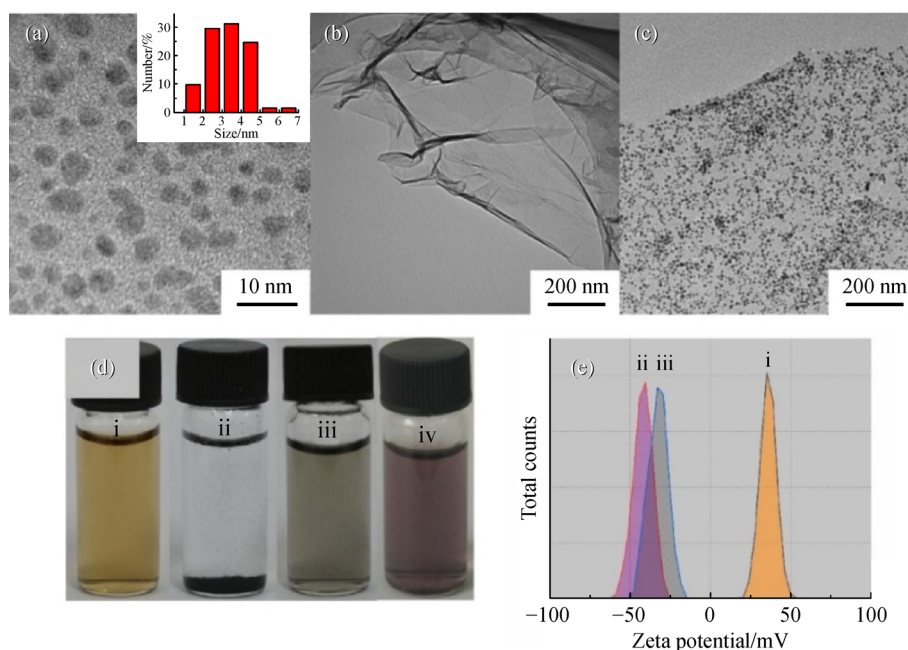


Fig. 1 TEM images of (a) AuNPs (inset: the corresponding size distribution histogram of AuNPs), (b) ssDNA-rGO and (c) AuNPs/ssDNA-rGO; (d) photos of (i) GO, (ii) rGO, (iii) ssDNA-rGO and (iv) AuNPs/ssDNA-rGO; (e) zeta potentials of (i) AuNPs, (ii) ssDNA-rGO and (iii) AuNPs/ssDNA-rGO.

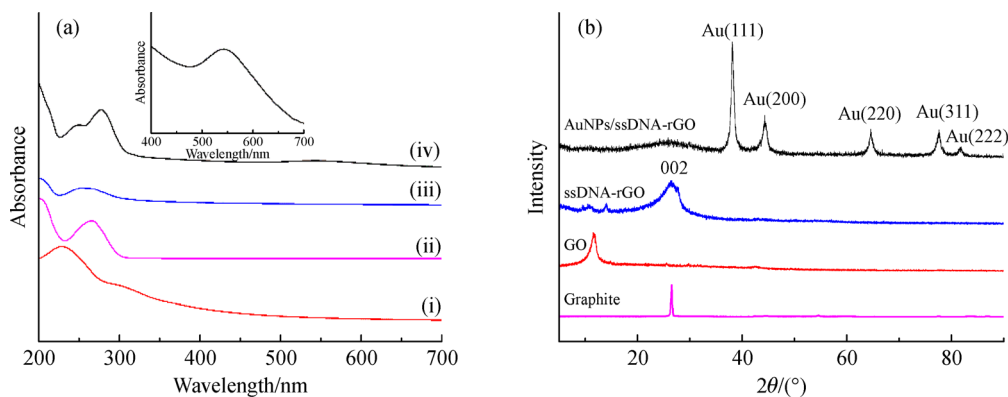


Fig. 2 (a) The UV-Vis spectrogram of GO (i), ssDNA-rGO (ii), ssDNA (iii) and AuNPs/ssDNA-rGO (iv) aqueous dispersions (inner illustration: enlarged UV-Vis curve of AuNPs/ssDNA-rGO); (b) XRD patterns of Graphite, GO, ssDNA-rGO and AuNPs/ssDNA-rGO.

on the layer spacing of rGO. Compared with ssDNA-rGO, AuNPs/ssDNA-rGO presented new diffraction peaks at 38.2° , 44.4° , 64.7° , 77.6° and 81.8° , respectively. Compared with JCPDS(04-0784) standard card, these diffraction peaks were the characteristic peaks of the cubic crystal system of Au(111), Au(200), Au(220), Au(311) and Au(222), respectively [38]. Thus, the AuNPs on rGO maintained a good crystal structure.

The preparation process of the ChOx/AuNPs/ssDNA-rGO nanocomposite modified electrode was illustrated schematically in Fig. 3. The GO was reduced *in situ* by hydrazine hydrate in the presence of ssDNA. ssDNA was modified to rGO nanosheets by a strong π - π interaction to form stable ssDNA-rGO hybrid. The modification of ssDNA could not only endow rGO with good biocompatibility and enhance water dispersion, but also increase the negative charges on the rGO surface. Based on the negative electric properties of ssDNA-rGO, the AuNPs with positive charges could be composited by electrostatic interaction. The AuNPs had good monodispersity due to the good adsorption and stabilization of ssDNA, resulting in the formation of the AuNPs/ssDNA-rGO nanocomposite with negative charges on the surface and better

electrical conductivity. The ChOx had a significant positive charge when pH is 4.0, and the ChOx/AuNPs/ssDNA-rGO/GCE was obtained by electrostatic adsorption self-assembly of the nanocomposite and ChOx.

3.2 Study on electrochemical performance of the ChOx/AuNPs/ssDNA-rGO/GCE

Figure 4 shows the alternating-current impedance spectra of different modified electrodes tested in the $5 \text{ mmol} \cdot \text{L}^{-1}$ of $\text{Fe}(\text{CN})_6^{3-/4-}$ solution. As could be seen, the impedance value of ssDNA-rGO/GCE was much smaller than that of the bare GCE, indicating that the conductivity of the electrode modified by the ssDNA-rGO was increased. Compared with the impedance value of ssDNA-rGO, the surface of ssDNA-rGO modified with AuNPs was further reduced, which illustrated the electron transfer rate was accelerated by the AuNPs, and the AuNPs successfully complexed with ssDNA-rGO. The impedance value increased significantly when ChOx was adsorbed onto AuNPs/ssDNA-rGO/GCE, owing to the ChOx was a non-conductive substance, which hindered the electronic transfer process.

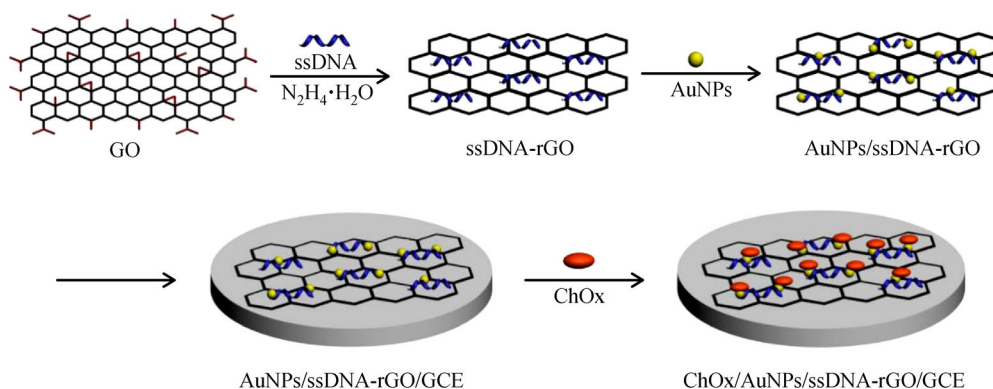


Fig. 3 Schematic illustration of the preparation process of ChOx/AuNPs/ssDNA-rGO/GCE.

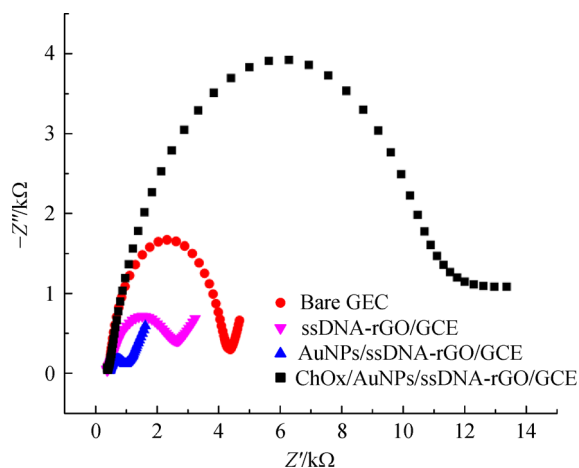


Fig. 4 Nyquist plots of bare GCE, ssDNA-rGO/GCE, AuNPs/ssDNA-rGO/GCE and ChOx/AuNPs/ssDNA-rGO/GCE in $5.0 \text{ mmol} \cdot \text{L}^{-1} \text{Fe}(\text{CN})_6^{3-/4-}$ solution containing $0.1 \text{ mol} \cdot \text{L}^{-1} \text{KCl}$.

3.3 Effect of pH value on the ChOx/AuNPs/ssDNA-rGO/GCE

Figure 5 shows the electrochemical behaviors of the immobilized ChOx influenced by the pH of PBS. Figure 5(a) is the CVs of the modified electrode in various pH values of PBS. As shown, the redox peaks of ChOx modified electrodes showed good reversibility at different pH values. With the increase of pH value, the potential peaks of anode and cathode were negatively shifted, indicating the electrochemical behaviors of the immobilized ChOx were affected by the pH. From the CV results in PBS with different pH values, the highest electrochemical response of the ChOx on the modified electrode was at pH 6.5. Based on this, the pH 6.5 PBS was selected as the supporting electrolyte for subsequent experiments. At the same time, the effect of pH on the formal potential was also studied. It could be seen from Fig. 5(b) that there was a linear relationship between the potential of

ChOx and the pH of PBS (4.0–8.0), and the slope was -53.0 mV/pH , testifying that the electrode reaction was equal protons and electrons process [39].

3.4 Direct electrochemistry of the ChOx/AuNPs/ssDNA-rGO/GCE

The electrochemical behaviors of ChOx/AuNPs/ssDNA-rGO/GCE were investigated by CVs and shown in Fig. S1 (cf. Electronic Supplementary Material, ESM). Figure S1(a) is the CVs of AuNPs/ssDNA-rGO/GCE and ChOx/AuNPs/ssDNA-rGO/GCE, respectively. As shown, there was no redox peak at AuNPs/ssDNA-rGO/GCE. However, a pair of obvious redox peaks appeared at ChOx/AuNPs/ssDNA-rGO/GCE, indicating that the AuNPs/ssDNA-rGO electrode had no electrochemical response within the range of such potential, and the direct electrochemistry could be realized between the immobilized ChOx and the surface of the electrode modified by AuNPs/ssDNA-rGO nanocomposites. Figure S1(b) shows the CVs of ChOx/AuNPs/ssDNA-rGO/GCE, ChOx/ssDNA-rGO/GCE and ChOx/AuNPs/ssDNA/GCE in N_2 saturated PBS, respectively. As shown, a pair of redox peaks appeared in all three modified electrodes, and the redox peak potentials were -0.360 , -0.407 , -0.359 , -0.408 , and -0.377 , -0.428 V , respectively. The peak difference was 47, 49 and 51 mV, and the potentials ($E^0 = (E_{\text{pa}} + E_{\text{pc}})/2$) were -0.384 , -0.382 and -0.403 V . According to the above results that the three modified electrodes could realize the direct electrochemistry of ChOx. However, under the same conditions, the peak current of ChOx/AuNPs/ssDNA-rGO/GCE was much larger than the others, and the potential difference was smaller. The CV curve of the modified electrode without rGO was not as good as which with rGO. The reduced conductivity of the nanocomposites resulted in a corresponding current reduction of the redox center of ChOx, illustrating that the AuNPs/ssDNA-rGO could better promote direct electron transfer between ChOx and

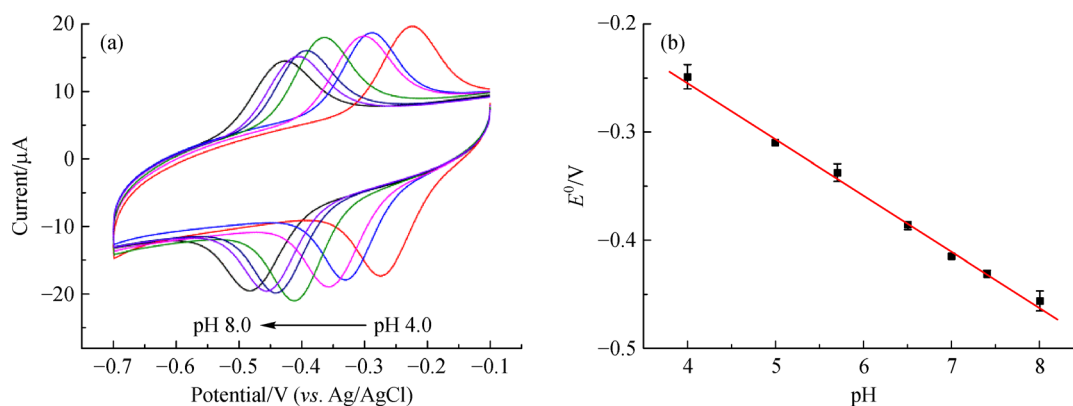


Fig. 5 (a) CVs of the ChOx/AuNPs/ssDNA-rGO/GCE in PBS at pH 4.0, 5.0, 5.7, 6.5, 7.0, 7.4 and 8.0, respectively (scan rate: $200 \text{ mV} \cdot \text{s}^{-1}$); (b) Plot of E^0 vs. pH.

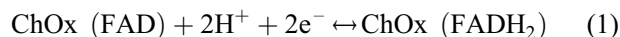
electrodes, which was presumed to be related to the good electrical conductivity and biocompatibility of AuNPs.

To investigate the kinetic behaviors of ChOx on the AuNPs/ssDNA-rGO/GCE, the change of redox peaks and linear relations at different scan rates of the modified electrodes were investigated by CVs (Fig. S2, cf. ESM). As shown in Fig. S2(a), the scan rates were in the range of $0.1\text{--}0.8\text{ V}\cdot\text{s}^{-1}$, and the peak currents of oxidation and reduction peaks increased with the augment of the scan rates, and changed linearly with the scan rates (Fig. S2(b)), manifesting that the electrochemical reaction process on the modified electrode was a surface-control process. The surface coverage (Γ^*) of ChOx adsorbed on AuNPs/ssDNA-rGO/GCE was calculated from Faraday's law $Q = nF\Gamma^*$ to be $5.11 \times 10^{-10}\text{ mol}\cdot\text{cm}^{-2}$, which was much larger than the reported value [40], also suggesting that the immobilized ChOx on the AuNPs/ssDNA-rGO nanocomposite film existed in a multi-layered state. The realization of the multilayer electron transfer process benefited from the large specific surface area, good biocompatibility and conductivity of the AuNPs/ssDNA-rGO nanocomposite, which increased the immobilization amount and maintained good biological activity of ChOx.

3.5 Catalytic performance of the ChOx/AuNPs/ssDNA-rGO/GCE for cholesterol

The catalytic performance of ChOx/AuNPs/ssDNA-rGO/GCE for cholesterol was studied by CV and DPV. The CVs of ChOx/AuNPs/ssDNA-rGO/GCE in N_2 saturated, containing $47.5\text{ }\mu\text{mol}\cdot\text{L}^{-1}$ cholesterol and O_2 saturated PBS, respectively, are shown in Fig. S3 (cf. ESM). There was a reversible redox peak under the condition of N_2 saturation, indicating that the ChOx immobilized on the surface of the electrode achieved their direct electron transfer. At the same time, it could be observed that under the condition of O_2 saturation, the reduction peak current was significantly increased because the ChOx participated in the redox

reaction, as shown in curve c. The reduced state of the coenzyme (FADH_2) was oxidized to the oxidation state (FAD). However, when cholesterol was added into the O_2 saturated PBS, the reduction peak current became smaller, demonstrating that the immobilized ChOx well catalyzed cholesterol. The catalytic mechanism was shown in Eqs. (1)–(3):



The DPVs and catalytic linear relationship of ChOx/AuNPs/ssDNA-rGO/GCE in PBS containing different concentrations of cholesterol are shown in Fig. 6. As the cholesterol concentration increased, the reduction peak currents of ChOx/AuNPs/ssDNA-rGO/GCE decreased accordingly (Fig. 6(a)), owing to the cholesterol in the solution was oxidized to 4-cholesten-3-ketone, and the oxidation state of ChOx(FAD) was reduced resulting in the decrease of the concentration of ChOx (FAD). The variation of the catalytic peak currents showed a good linear relationship with cholesterol concentration in the concentration range of $7.5\text{--}280.5\text{ }\mu\text{mol}\cdot\text{L}^{-1}$ (Fig. 6(b)), and the linear equation was $y = 0.043x + 9.934$ (x was the concentration of cholesterol, y represented the response currents), the linear correlation coefficient R^2 was 0.998 ($n = 18$), and the limit of detection (LOD) was calculated to be $2.1\text{ }\mu\text{mol}\cdot\text{L}^{-1}$ according to the $\text{LOD} = 3\sigma/S$ (where σ represents the standard deviation of peak currents of the blanks and S represents the slope of calibration plot) [41]. According to the slope of the calibration curve, the sensitivity of the modified electrode was $0.61\text{ }\mu\text{A}\cdot\mu\text{L}\cdot\text{mol}^{-1}\cdot\text{cm}^{-2}$.

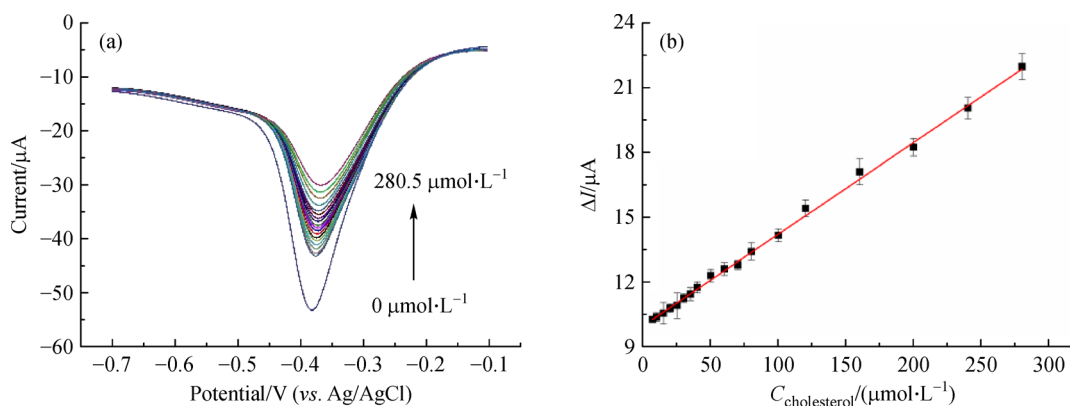


Fig. 6 (a) DPVs of ChOx/AuNPs/ssDNA-rGO/GCE in $0.1\text{ mol}\cdot\text{L}^{-1}$ O_2 -saturated PBS (pH 6.5) in the presence of different concentrations of 0, 7.5, 10.5, 15.5, 20.5, 25.5, 30.5, 35.5, 40.5, 50.5, 60.5, 70.5, 80.5, 100.5, 120.5, 160.5, 200.5, 240.5, $280.5\text{ }\mu\text{mol}\cdot\text{L}^{-1}$ cholesterol; (b) plot of the catalytic currents (ΔI) vs. cholesterol concentration.

3.6 Anti-interference ability of the ChOx/AuNPs/ssDNA-rGO/GCE

The effects of some interfering substances in serum coexisting with cholesterol were examined. As illustrated in Fig. 7, the peak currents weren't significantly changed when the coexisted interferences of 0.1 mmol·L⁻¹ AA, UA, LA and Glu [42], respectively were added to PBS containing 40 μmol·L⁻¹ cholesterol. Then, when the cholesterol was added, the peak current changed obviously, illustrating that the ChOx/AuNPs/ssDNA-rGO/GCE had good selectivity for cholesterol.

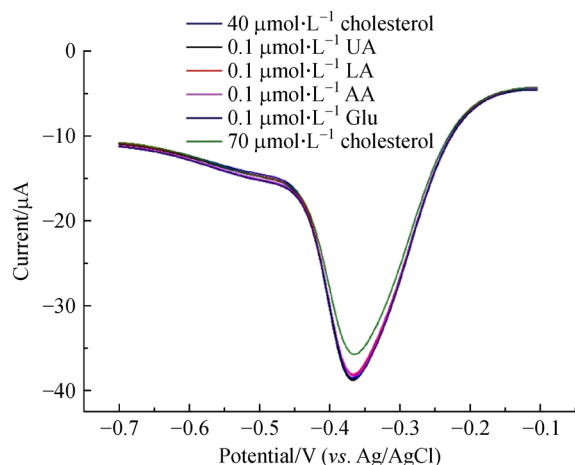


Fig. 7 DPVs of ChOx/AuNPs/ssDNA-rGO/GCE in 0.1 mol·L⁻¹ O₂-saturated PBS (pH 6.5) in the presence of 40 μmol·L⁻¹ cholesterol, 0.1 mmol·L⁻¹ UA, 0.1 mmol·L⁻¹ LA, 0.1 mmol·L⁻¹ AA, 0.1 mmol·L⁻¹ Glu and 70 μmol·L⁻¹ cholesterol.

3.7 Reproducibility and stability of the ChOx/AuNPs/ssDNA-rGO/GCE

The reproducibility of the ChOx/AuNPs/ssDNA-rGO/GCE was studied. Six as-prepared modified electrodes

were used to determine 30 μmol·L⁻¹ cholesterol. The relative standard deviation of response currents was 2.5%, indicating ChOx/AuNPs/ssDNA-rGO/GCE had good repeatability.

In addition, the stability of ChOx/AuNPs/ssDNA-rGO/GCE was also investigated, and the effect of storage time on the stability of ChOx/AuNPs/ssDNA-rGO/GCE was studied. The modified electrodes were stored in the refrigerator at 4 °C for 5 d and 10 d, and the response currents were 98% and 96% of the initial values, respectively, showing good long-term stability, which might be attributed to the good biocompatibility of the AuNPs and the good biological activity of ChOx maintained by ssDNA-rGO. Compared to the other reported cholesterol biosensors based on ChOx and nanomaterials, the as-prepared biosensor exhibited higher sensitivity, lower detection limit and good stability (Table 1).

3.8 Real sample analysis

To evaluate the potential applicability of the proposed biosensor for cholesterol detection in complex biological samples, the determination of cholesterol in human blood serum had been examined. The serum samples donated by local hospital were pre-treated with ChEt to hydrolyze the esterified cholesterol into free cholesterol [48] and were diluted (1:200) with PBS before detection. The content of spiked cholesterol in human blood serum was also investigated [49]. The standard addition method was carried out to test the recovery of the proposed biosensor, the analyte samples (an appropriate cholesterol standard solution) were added to the cell and the DPV responses were recorded, respectively. The values of the recovery obtained were in the range of 96.0%–104.0%. The obtained results (Table S1, cf. ESM) indicated that the analyses for cholesterol in serum samples were acceptable and reliable.

Table 1 Comparison of different cholesterol electrochemical biosensors

Electrode	Detection method	Detection of limit / (μmol·L ⁻¹)	Linear range / (μmol·L ⁻¹)	R ²	Sensitivity / (μA ⁻¹ ·mL ⁻¹ ·mol ⁻¹ ·cm ⁻²)	Stability	Ref.
CoMnHCF/Nafion/ChOx ^{a)}	CV	30	50–150 150–1000	0.99 0.97	385 80	–	[43]
PPy-NO ₃ ⁻ -Fe(CN) ₆ ⁴⁻ -AuNPs- COx-CE ^{b)}	Amperometry	–	25–170	0.972	100	30 d (30%)	[17]
ChOx-gRGO-PPy/GCE ^{c)}	DPV	3.78	10–6000	0.99	1095.3	7 d (96%)	[44]
GCE/PTH/ChOx/HRP ^{d)}	DPV	6.3	25–125	0.99	180	30 d (90%)	[45]
G/Ti(G)-3DNS/CS/ChOx bioelectrode ^{e)}	CV	6.0	50–8000	0.99	3.82	5 d (>98%)	[46]
ChOx/Pt/rGO/P3ABA/SPE ^{f)}	Amperometry	40.5	250–4000	0.993	15.94	7 d (88%)	[47]
PEI/(ChOx/PEI-rGO) ₃ /GCE	DPV	2.1	7.5–280.5	0.998	610	10 d (96%)	Present work

a) Hexacyanoferrate(III) containing Co²⁺ and Mn²⁺/Nafion/ChOx; b) pyrrole-NO₃⁻-Fe(CN)₆⁴⁻-gold nanoparticles-cholesterol oxidase-cholesterol esterase; c) ChOx-green reduced graphene oxide-polypyrrole/GCE; d) GCE/poly(thionine)/ChOx/horseradish peroxidase; e) graphene/graphene embedded titanium nanowires (TiO₂(G)-NWs) 3D nanostacks/chitosan/ChOx bioelectrode; f) ChOx/platinum/reduced graphene oxide/poly(3-aminobenzoic acid)/screen-printed carbon electrode.

4 Conclusions

In summary, a high selective and sensitive cholesterol electrochemical biosensor was fabricated for cholesterol detection based on AuNPs/ssDNA-RGO nanocomposites. The results showed that the AuNPs/ssDNA-rGO nanocomposites enabled ChOx to achieve direct electron transmission and enhanced the performance of fabricated biosensors with high sensitivity, low detection limit, good selectivity, stability, and reproducibility, which was benefited from the large surface area, excellent biocompatibility, fast electron transport, and synergistic effect of AuNPs and ssDNA-rGO. The excellent performance of ChOx/AuNPs/ssDNA-rGO/GCE demonstrated that it would be a promising biosensor for the electrochemical detection of cholesterol. The as-prepared nanocomposites might provide an alternative platform for the detection of other biomolecules only by changing the enzyme.

Acknowledgements The authors gratefully acknowledge financial support from the National Natural Science Foundation of China (Grant Nos. 51773085, 52071171), the Liaoning Province Doctor Start-up Fund (Grant No. 20170520282) and the Doctor Start-up Fund of Liaoning University (Grant No. a280008020), research fund pre-declaration project of Liaoning University (Grant No. LDGY2019001), teaching reform research project of Liaoning University (Grant Nos. JG2018YB20, LNDXJG20183013, JG2020ZSWT022), Liaoning Revitalization Talents Program—Pan Deng Scholars (Grant No. XLYC1802005), Liaoning BaiQianWan Talents Program (Grant No. LNBQW2018B0048), Natural Science Fund of Liaoning Province for Excellent Young Scholars (Grant No. 2019-YQ-04), and Key Project of Scientific Research of the Education Department of Liaoning Province (Grant No. LZD201902), the Young Scientific and Technological Talents Project of the Department of Education of Liaoning Province (Grant Nos. LQN201903 and LQN202008), the Foundation for Young Scholars of Liaoning University (Grant No. LDQN2019007).

Electronic Supplementary Material Supplementary material is available in the online version of this article at <https://doi.org/10.1007/s11705-021-2112-4> and is accessible for authorized users.

References

1. Ikonen E. Cellular cholesterol trafficking and compartmentalization. *Nature Reviews. Molecular Cell Biology*, 2008, 9(2): 125–138
2. Huang Y, Tan J, Cui L, Zhou Z, Zhou S, Zhang Z, Zheng R, Xue Y, Zhang M, Li S, et al. Graphene and Au NPs co-mediated enzymatic silver deposition for the ultrasensitive electrochemical detection of cholesterol. *Biosensors & Bioelectronics*, 2018, 102: 560–567
3. Sekretaryova A N, Beni V, Eriksson M, Karyakin A A, Turner A P F, Vagin M Y. Cholesterol self-powered biosensor. *Analytical Chemistry*, 2014, 86(19): 9540–9547
4. Yang L, Zhao H, Li Y, Ran X, Deng G, Zhang Y, Ye H, Zhao G, Li C P. Indicator displacement assay for cholesterol electrochemical sensing using a calix[6]arene functionalized graphene-modified electrode. *Analyst (London)*, 2016, 141(1): 270–278
5. Li L, Wang Y, Pan L, Shi Y, Cheng W, Shi Y, Yu G. A nanostructured conductive hydrogels-based biosensor platform for human metabolite detection. *Nano Letters*, 2015, 15(2): 1146–1151
6. Nantaphol S, Chailapakul O, Siangproh W. Sensitive and selective electrochemical sensor using silver nanoparticles modified glassy carbon electrode for determination of cholesterol in bovine serum. *Sensors and Actuators. B, Chemical*, 2015, 207: 193–198
7. Gorassini A, Verardo G, Fregolent S C, Bortolomeazzi R. Rapid determination of cholesterol oxidation products in milk powder based products by reversed phase SPE and HPLC-APCI-MS/MS. *Food Chemistry*, 2017, 230: 604–610
8. Chitra J, Ghosh M, Mishra H N. Rapid quantification of cholesterol in dairy powders using Fourier transform near infrared spectroscopy and chemometrics. *Food Control*, 2017, 78: 342–349
9. Galdino N M, Brehm G S, Bussamara R, Gonçalves W D G, Abarca G, Scholten J D. Sputtering deposition of gold nanoparticles onto graphene oxide functionalized with ionic liquids: biosensor materials for cholesterol detection. *Journal of Materials Chemistry. B, Materials for Biology and Medicine*, 2017, 5(48): 9482–9486
10. Chen A, Chatterjee S. Nanomaterials based electrochemical sensors for biomedical applications. *Chemical Society Reviews*, 2013, 42(12): 5425–5438
11. Abdi M M, Razalli R L, Tahir P M, Chaibakhsh N, Hassani M, Mir M. Optimized fabrication of newly cholesterol biosensor based on nanocellulose. *International Journal of Biological Macromolecules*, 2019, 126: 1213–1222
12. Rison S, Akshaya K B, Bhat V S, Shanker G, Varghese A. MnO₂ nanoclusters decorated on graphene modified pencil graphite electrode for non-enzymatic determination of cholesterol. *Electroanalysis*, 2020, 32(10): 1–10
13. Saxena U, Das A B. Nanomaterials towards fabrication of cholesterol biosensors: key roles and design approaches. *Biosensors & Bioelectronics*, 2016, 75: 196–205
14. Gao J, Huang W, Chen Z, Yi C, Jiang L. Simultaneous detection of glucose, uric acid and cholesterol using flexible microneedle electrode array-based biosensor and multi-channel portable electrochemical analyzer. *Sensors and Actuators. B, Chemical*, 2019, 287: 102–110
15. Garcia Raya D, Silien C, Blazquez M, Pineda T, Madueno R. Electrochemical and AFM study of the 2D-assembly of colloidal gold nanoparticles on dithiol sams tuned by ionic strength. *Journal of Physical Chemistry C*, 2014, 118(26): 14617–14628
16. Ng B Y C, Xiao W, West N P, Wee E J H, Wang Y, Trau M. Rapid, single-cell electrochemical detection of mycobacterium tuberculosis using colloidal gold nanoparticles. *Analytical Chemistry*, 2015, 87(20): 10613–10618
17. Rahim M Z A, Govender-Hondros G, Adeloju S B. A single step electrochemical integration of gold nanoparticles, cholesterol oxidase, cholesterol esterase and mediator with polypyrrole films for fabrication of free and total cholesterol nanobiosensors. *Talanta*, 2018, 189: 418–428
18. Han Y, Zhang R, Dong C, Cheng F, Guo Y. Sensitive electrochemical sensor for nitrite ions based on rose-like AuNPs/MoS₂/graphene composite. *Biosensors & Bioelectronics*, 2019, 142: 111529
19. Kumar-Krishnan S, Guadalupe-Ferreira Garcia M, Prokhorov E, Estevez-González M, Pérez R, Esparza R, Meyyappan M. Synthesis of gold nanoparticles supported on functionalized nanosilica using deep eutectic solvent for an electrochemical enzymatic glucose

- biosensor. *Journal of Materials Chemistry. B, Materials for Biology and Medicine*, 2017, 5(34): 7072–7081
20. Yuan R, Cao S R, Chai Y Q, Gao F X, Zhao Q, Tang M Y, Tong Z Q, Xie Y. Direct electrochemistry and enzymatic activity of hemoglobin in positively charged colloid Au nanoparticles and hemoglobin layer-by-layer self-assembly films. *Science China. Chemistry*, 2007, 50(5): 620–628
 21. Lu Z W, Li Y F, Liu T, Wang G T, Sun M M, Jiang Y Y, He H, Wang Y Y, Zou P, Wang X X, et al. A dual-template imprinted polymer electrochemical sensor based on AuNPs and nitrogen-doped graphene oxide quantum dots coated on NiS₂/biomass carbon for simultaneous determination of dopamine and chlorpromazine. *Chemical Engineering Journal*, 2020, 389: 124417–124426
 22. Zhai H, Wang H, Wang S, Chen Z, Wang S, Zhou Q, Pan Y. Electrochemical determination of mangiferin and icariin based on Au-AgNPs/MWNTs-SGSs modified glassy carbon electrode. *Sensors and Actuators. B, Chemical*, 2018, 255: 1771–1780
 23. Geim A K, Novoselov K S. The rise of graphene. *Nature Materials*, 2007, 6(3): 183–191
 24. Bo X, Zhou M, Guo L. Electrochemical sensors and biosensors based on less aggregated graphene. *Biosensors & Bioelectronics*, 2017, 89(Pt 1): 167–186
 25. Ambrosi A, Chua C K, Latiff N M, Loo A H, Wong C H A, Eng A Y S, Bonanni A, Pumera M. Graphene and its electrochemistry—an update. *Chemical Society Reviews*, 2016, 45(9): 2458–2493
 26. Jiang J, Ding D, Wang J, Lin X, Diao G. Three-dimensional nitrogen-doped graphene-based metal-free electrochemical sensors for simultaneous determination of ascorbic acid, dopamine, uric acid, and acetaminophen. *Analyst (London)*, 2021, 146(3): 964–970
 27. Fritea L, Tertis M, Sandulescu R, Cristea C. Chapter eleven. Enzyme-graphene platforms for electrochemical biosensor design with biomedical applications. In: Kumar C V, ed. *Methods in Enzymology*. Massachusetts: Academic Press, 2018, 293–333
 28. Wu S, Hao J, Yang S, Sun Y, Wang Y, Zhang W, Mao H, Song X M. Layer-by-layer self-assembly film of PEI-reduced graphene oxide composites and cholesterol oxidase for ultrasensitive cholesterol biosensing. *Sensors and Actuators. B, Chemical*, 2019, 298: 126856–126864
 29. Wu S Y, Wang Y X, Mao H, Wang C, Xia L X, Zhang Y, Ge H, Song X M. Direct electrochemistry of cholesterol oxidase and biosensing of cholesterol based on PSS/polymeric ionic liquid-graphene nanocomposite. *RSC Advances*, 2016, 6(64): 59487–59496
 30. Patil A J, Vickery J L, Scott T B, Mann S. Aqueous stabilization and self-assembly of graphene sheets into layered bio-nanocomposites using DNA. *Advanced Materials*, 2010, 21(31): 3159–3164
 31. Xu Z, Lei X, Tu Y, Tan Z J, Song B, Fang H. Dynamic cooperation of hydrogen binding and π stacking in ssDNA adsorption on graphene oxide. *Chemistry (Weinheim an der Bergstrasse, Germany)*, 2017, 23(53): 13100–13104
 32. Zhang Q, Qiao Y, Hao F, Zhang L, Wu S, Li Y, Li J, Song X M. Fabrication of a biocompatible and conductive platform based on a single-stranded DNA/graphene nanocomposite for direct electrochemistry and electrocatalysis. *Chemistry (Weinheim an der Bergstrasse, Germany)*, 2010, 16(27): 8133–8139
 33. Patil A, Vickery J, Scott T, Mann S. Aqueous stabilization and self-assembly of graphene sheets into layered bio-nanocomposites using DNA. *Advanced Materials*, 2009, 21(31): 3159–3164
 34. Jr Hummers W S, Offeman R E. Preparation of graphitic oxide. *Journal of the American Chemical Society*, 1958, 80(6): 1339
 35. Gittins D I, Caruso F. Spontaneous phase transfer of nanoparticulate metals from organic to aqueous media. *Angewandte Chemie International Edition*, 2001, 40(16): 3001–3004
 36. Dikmen S, Yılmaz G, Yörükoğulları E, Korkmaz E. Zeta potential study of natural- and acid-activated sepiolites in electrolyte solutions. *Canadian Journal of Chemical Engineering*, 2012, 90(3): 785–792
 37. Zhang Q, Wu S, He M, Zhang L, Liu Y, Li J, Song X M. Preparation and bioelectrochemical application of gold nanoparticles-chitosan-graphene nanomaterials. *Acta Chimica Sinica*, 2012, 70(21): 2213–2219
 38. Zhang Y, Li X, Li D, Wei Q. A laccase based biosensor on AuNPs-MoS₂ modified glassy carbon electrode for catechol detection. *Colloids and Surfaces. B, Biointerfaces*, 2020, 186: 110683–110690
 39. Li X R, Xu J J, Chen H Y. Potassium-doped carbon nanotubes toward the direct electrochemistry of cholesterol oxidase and its application in highly sensitive cholesterol biosensor. *Electrochimica Acta*, 2011, 56(25): 9378–9385
 40. Zhu L, Xu L, Tan L, Tan H, Yang S, Yao S. Direct electrochemistry of cholesterol oxidase immobilized on gold nanoparticles-decorated multiwalled carbon nanotubes and cholesterol sensing. *Talanta*, 2013, 106: 192–199
 41. Rashidi K, Mahmoudi M, Mohammadi G, Zangeneh M M, Korani S, Goicoechea H C, Gu H W, Jalalvand A R. Simultaneous co-immobilization of three enzymes onto a modified glassy carbon electrode to fabricate a high-performance amperometric biosensor for determination of total cholesterol. *International Journal of Biological Macromolecules*, 2018, 120(Pt A): 587–595
 42. Thakur N, Kumar M, Das Adhikary S, Mandal D, Nagaiah T C. PVIM-Co₃POM/MNC composite as a flexible electrode for the ultrasensitive and highly selective non-enzymatic electrochemical detection of cholesterol. *Chemical Communications*, 2019, 55(34): 5021–5024
 43. Antuch M, Matos-Peralta Y, Llanes D, Echevarría F, Rodríguez-Hernández J, Marin M H, Díaz-García A M, Reguera L. Bimetallic Co²⁺ and Mn²⁺ hexacyanoferrate for hydrogen peroxide electro-oxidation and its application in a highly sensitive cholesterol biosensor. *ChemElectroChem*, 2019, 6(5): 1567–1573
 44. Pramanik K, Sarkar P, Bhattacharyay D, Majumdar P. One step electrode fabrication for direct electron transfer cholesterol biosensor based on composite of polypyrrole, green reduced graphene oxide and cholesterol oxidase. *Electroanalysis*, 2018, 30(11): 2719–2730
 45. Rahman M M, Li X B, Kim J, Lim B O, Ahammad A J S, Lee J J. A cholesterol biosensor based on a bi-enzyme immobilized on conducting poly(thionine) film. *Sensors and Actuators. B, Chemical*, 2014, 202: 536–542
 46. Komathi S, Muthuchamy N, Lee K P, Gopalan A I. Fabrication of a novel dual mode cholesterol biosensor using titanium dioxide nanowire bridged 3D graphene nanostacks. *Biosensors & Bioelectronics*, 2016, 84: 64–71

47. Phetsang S, Jakmunee J, Mungkornasawakul P, Laocharoensuk R, Ounnunkad K. Sensitive amperometric biosensors for detection of glucose and cholesterol using a platinum/reduced graphene oxide/poly(3-aminobenzoic acid) film-modified screen-printed carbon electrode. *Bioelectrochemistry (Amsterdam, Netherlands)*, 2019, 127: 125–135
48. Yang D P, Guo W, Cai Z, Chen Y, He X, Huang C, Zhuang J, Jia N. Highly sensitive electrochemiluminescence biosensor for cholesterol detection based on AgNPs-BSA-MnO₂ nanosheets with superior biocompatibility and synergistic catalytic activity. *Sensors and Actuators. B, Chemical*, 2018, 260: 642–649
49. Wu Q, He L, Jiang Z W, Li Y, Cao Z M, Huang C Z, Li Y F. CuO nanoparticles derived from metal-organic gel with excellent electrocatalytic and peroxidase-mimicking activities for glucose and cholesterol detection. *Biosensors & Bioelectronics*, 2019, 145: 111704